JOURNAL OF AIRCRAFT
Vol. 37, No. 4, July–August 2000

Engineering Notes

ENGINEERING NOTES are short manuscripts describing new developments or important results of a preliminary nature. These Notes cannot exceed 6 manuscript pages and 3 figures; a page of text may be substituted for a figure and vice versa. After informal review by the editors, they may be published within a few months of the date of receipt. Style requirements are the same as for regular contributions (see inside back cover).

Tailoring Lift/Drag Ratio for a Lifting-Body Airplane Configuration

Joseph Katz* and Bernhard Roglin†
San Diego State University, San Diego, California 92182

Introduction

A LIFTING-BODY/WING airplane configuration can, in principle, generate high lift coefficients by utilizing fuselage lift, reducing the need for multielement, high-lift systems upon takeoff and landing. Previous small-scale wind-tunnel data[1] on a generic lifting-body/wing configuration, having a much wider body than the usual cylindrical shape, indicated that this approach could yield an efficient airplane with distinct advantages in passenger comfort because of larger cabin volume. A pronounced stall-resistant behavior was also noted, which might be tailored to create a sharp increase in the nose-down pitching moment at high angles of attack, providing an aerodynamically stall-safe airplane. The previous wind-tunnel model,[1] a 1:20 scale replica of a generic business jet, had an untwisted NASA 410M6 transonic airfoil section, shown schematically in Fig. 1. Because of the low Reynolds number of the test[1] (near 400,000), the wing stalled at about 5 deg angle of attack, much earlier than a full-scale airplane would have been expected to stall. While demonstrating the basic stall-resistant feature of the configuration, the model did not demonstrate the high lift/drag (L/D) ratio potential of the lifting-body concept because of this early wing-stall problem.

An objective of the present study was to partially simulate full-scale conditions by modifying the wing airfoil shape so that it would stall in the range expected of a full-scale aircraft. Two[2]- and three[3]-dimensional computational tools were used to develop an airfoil section with a target stall angle of attack α above 14 deg. The modified airfoil shape is shown below the NASA 410M6 airfoil shape in Fig. 1, and its target stall angle was verified experimentally (within $\alpha = \pm 0.5$ deg). Tailoring the airfoil design to the test Reynolds number served to demonstrate the high L/D-ratio potential of such lifting-body/wing configurations, without compromising the stall-resistant feature. Additionally, these two airfoil shapes can be viewed as the two extreme geometries of an adaptive wing, transforming from the cambered airfoil shape at takeoff into the transonic section at cruise.

Model Design and Test Procedure

The basic dimensions of the models are shown in Fig. 1. From the side view the lifting-body is defined by an 18% thick NACA 633-018 airfoil section, with maximum thickness at 35% of the length measured from the nose. At this maximum thickness location the body has an aspect-ratio 2.2, elliptic cross section (from the front view). In the top view the nose shape follows the contours of a semi-ellipse up to the 35% length point, and from thereon the fuselage has a constant width to the tail. The same body used in the previous study[1] was fitted with a new wing, using the modified airfoil. The fuselage geometry and wing-sweep angle were kept the same with no wing twist, but the wing aspect ratio and airfoil shape were modified. Because the primary concern was improving L/D, wing aspect ratio was increased from 8.26 to 12.38, but wing area was kept about the same (the new wing area was 0.7% smaller). Thus, the reference area of $A_R = 831$ cm^2 was kept the same as in Ref. 1, but a smaller reference chord of $c_R = 9.5$ cm was used, compared with $c_R = 11.2$ cm in Ref. 1. Also, the total wetted surface area of the model was 4.507 times larger than the preceding reference area.

The new airfoil shape was developed by using a two-dimensional airfoil design code,[2] which was combined with a three-dimensional panel code[3] to model the complete configuration. A stall angle above $\alpha = 14$ deg was specified so that the maximum L/D ratio could be obtained with a fully attached flow on the wings at the test Reynolds number. The airfoil geometry was initially developed by using the inverse mode of the two-dimensional code,[2] which was then transferred to the three-dimensional panel code[3] to verify the effect of the three-dimensional flow on the pressure distribution. These effects could be characterized as an angle-of-attack correction for most parts of this high aspect ratio wing, excluding the root and tip regions. After several iterations the airfoil shape shown at the bottom of Fig. 1 and in Fig. 2 was obtained. Because of the desirable high angle-of-attack stall at this low Reynolds number (0.4×10^6), quite a large camber was required. During wind-tunnel tests, the flow seemed to be attached on the wing's upper surface, up to angles of attack of $\alpha = 14$ deg. At $\alpha = 15$ deg a trailing-edge separation

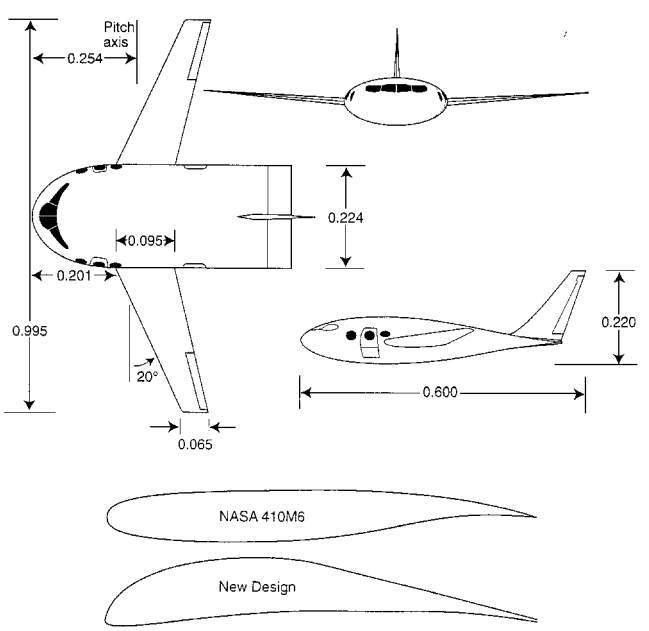

Fig. 1 Basic dimensions of the lifting-body model. The airfoil section used in Ref. 1 (upper) and the new airfoil used for this study (lower) are shown at the bottom of the figure.

Received 28 February 1999; revision received 5 February 2000; accepted for publication 4 April 2000.

*Professor, Department of Aerospace Engineering and Engineering Mechanics. Associate Fellow AIAA.

†Graduate Student, Department of Aerospace Engineering and Engineering Mechanics.

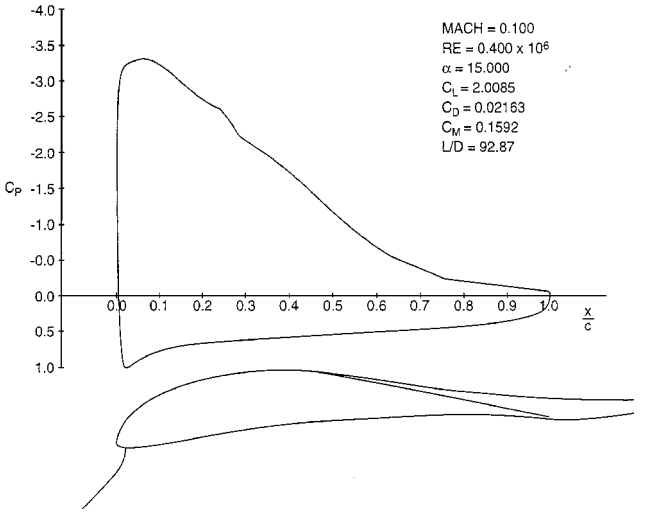

Fig. 2 Two-dimensional computations[2] showing the pressure distribution and separating streamline on the airfoil ($Re = 0.4 \times 10^6$, $\alpha = 15$ deg).

developed and was visible when using tufts in the wind tunnel. Sample computational results[2] for this condition are presented in Fig. 2, showing about 25% trailing-edge separation. Also a discontinuity, possibly caused by a laminar bubble, at about 25% of the upper surface is shown by the computations (with calculated transition beginning at about 20% chord).

Wind-tunnel test-section dimensions were 0.91 m height × 1.22 m width, with frontal blockage of less than 2%, at lower incidence, increasing slightly above 4% at angles of attack over 20 deg. Therefore, no blockage corrections were applied to the data presented here. Wind-tunnel air speed was set at 45 m/s resulting in a wing chord-based Reynolds number of about 0.4×10^6. Freestream turbulence levels were less than 0.5%, and without boundary-layer tripping devices free transition on the wings and fuselage can be assumed. Estimated uncertainty of the data, including the accuracy of the six-component scale, air-speed measurements errors, and data reduction system uncertainties, is less than $C_L = \pm 0.01$, $C_D = \pm 0.005$, and $C_M = \pm 0.01$.

Results

Comparisons between the L/D coefficients of the present configuration and the one tested in Ref. 1 are presented in Fig. 3. The major effects of the wing modifications were in delaying the wing stall and shifting the drag polar to higher angles of attack. The angle of attack for both models (present and of Ref. 1) was measured relative to the body's centerline. For example, at $\alpha = 0$ the lift coefficient for the preceding configuration was about $C_L = 0.22$, yielding a zero lift angle of about -1.5 deg; compared with $C_L \sim 0.0$ at $\alpha = 0$ for the present case, indicating a slight change in the wing's relative incidence. The slope of the preceding configuration's lift coefficient, depicted by the circular symbols, changes at about $\alpha = 5$ deg as a result of the wing stall. This is a result of the transonic airfoil design and the low Reynolds number of the small-scale test. In spite of this problem, the configuration lift coefficient increases up to and beyond $\alpha = 18$ deg because of the vortex lift of the aft section of the fuselage (see Ref. 1). Because of the early wing stall, the drag coefficient of the preceding configuration (solid triangular symbols) increases sharply above $\alpha = 5$ deg.

The present configuration (lift depicted by the rectangular symbols) actually creates lower lift and higher drag (solid diamond symbols) coefficients at angles of attack below $\alpha = 5$ deg because of the high airfoil camber. In fact, minimum drag (of about $C_D = 0.035$) is obtained at about $\alpha = 5$ deg compared to $C_D = 0.025$ near $\alpha = 0$ deg for the preceding design. At larger angles of attack, however, the flow is attached, and the lift increases up to $\alpha = 21$ deg, though wing trailing-edge stall occurs for $\alpha > 14$ deg (based on flow visualizations). Consequently, the drag of the present configuration, within the range of 5 deg $< \alpha <$ 22 deg, is considerably less than the drag

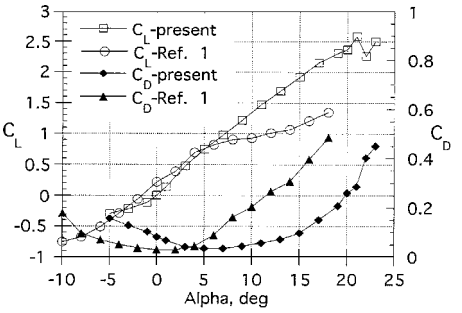

Fig. 3 Comparison of measured lift and drag vs angle of attack for the old[1] and present lifting body models ($Re = 0.4 \times 10^6$).

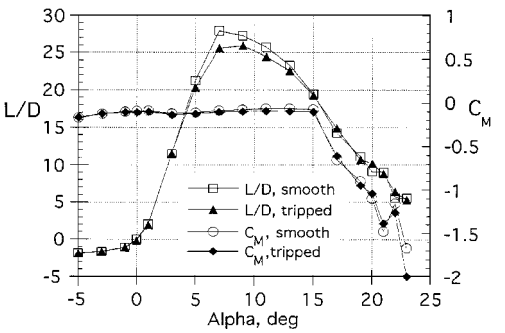

Fig. 4 Measured L/D and pitching moment variation vs angle of attack, with and without boundary-layer tripping on the fuselage ($Re = 0.4 \times 10^6$).

of the preceding model. Also, the change in the lift coefficient slope near the wing stall ($\alpha = 15$ deg) is less pronounced because of the gradual trailing-edge stall and the increase in the fuselage side-edge vortex lift. As a result, the lift coefficient of the complete configuration increases up to $\alpha = 21$ deg, reaching a level of $C_L \sim 2.6$, which is quite high considering there is no multielement high-lift system. The two sets of data in this figure can be viewed as the cruise and the high-lift ends of a possible flexible airfoil design, with the transition between the two airfoil shapes taking place at about $\alpha = 4$ deg.

The L/D ratio and pitching moment data vs angle of attack are presented in Fig. 4. As noted earlier, one of the primary objectives of the study was to prove that by delaying wing stall, considerably higher L/D ratios could be obtained than the value of L/D = 16 reported in Ref. 1. Indeed, the data in Fig. 4 demonstrate that the L/D ratio was greatly improved with the modified wing and reached a maximum value of L/D = 27.9. Because the model surface had a smooth finish (sanded and painted fiberglass), the relatively high L/D ratio could have been caused by large laminar flow regions on the fuselage (maximum fuselage thickness occurs at 35% length); therefore, the effect of tripping the fuselage boundary layer was briefly investigated. Boundary-layer tripping was obtained by placing stripes of sanding paper with grit size, the size of the expected boundary-layer thickness. To initiate boundary-layer transition, those stripes were placed around the model nose, between 5–10% of the fuselage length. A similar tripping of the wing boundary layer was not used because the two-dimensional computations showed quite early transition (as in Fig. 2, for $\alpha > 5$ deg) on this highly cambered airfoil. It seemed, though, that the tripping had very little effect, primarily increasing the drag (not shown here) and resulting in a slight decrease in the L/D ratio as shown by Fig. 4. This smaller than expected change in the drag can be attributed to the high prevailing turbulence levels in the wind-tunnel test section.

The L/D ratio of the present configuration (shown in Fig. 4) increases rapidly as angle of attack increases above $\alpha = 0$ deg, reaching a maximum at about $\alpha = 6$ deg. At larger angles of attack, the drag increases quicker than the lift (see C_D data in Fig. 3), probably because of the formation of fuselage side edge vortices and because of the wing boundary-layer effects, causing a rapid drop in the L/D ratio. For a particular mission, such as cruise condition, L/D can

be further improved by aligning the body with the freestream direction. For example, based on Fig. 4 and using a designed cruise lift coefficient of about $C_L = 1.0$, wing incidence can be increased to 6 deg relative to the fuselage to obtain L/D ratios higher than 27.9, and much higher than the reported L/D = 23 of some advanced configurations.[4,5]

The pitching moment data for the smooth and tripped fuselage-boundary layer flows are presented in Fig. 4, and the differences between these two cases are quite small. With the tripped boundary layer a slight increase in the nose-down moment was measured, particularly within the visually attached airfoil-flow region (5 deg $< \alpha <$ 14 deg). This incremental effect is caused by the slightly increased drag on the rougher surface, which also causes a small reduction in the lift. The most dominant feature of the pitching moment curve in Fig. 4 is the sharp increase in the nose-down moment beyond wing stall ($\alpha >$ 15 deg). At the lower angles of attack, however, the pitching moment in the present test was quite independent of α (near a value of $C_M = -0.1$), contrary to the continuous negative slope of the data in Ref. 1. The present and perhaps more desirable location for the pitch axis is a result of the modified wing geometry and some other minor model mounting changes in the wind-tunnel setup. The very large nose-down moment beyond wing stall, shown in this figure, is a result of the lift created by the aft-fuselage side-edge vortices. As noted in Ref. 1, this large increase in the negative slope of C_M can be considered as a stall resistant feature with important safety-related implications. Therefore, when airplane c.g. calculations and elevator sizing are complete, the use of these data can make airplane stall unreachable (note that effects such as fuselage side-edge vortex burst are delayed beyond $\alpha >$ 30 deg). For example, the pitching moment data presented in Ref. 1 show that the trailing-edge flap (elevator) is capable of creating a change of $\Delta C_M \sim 0.3$, which is much smaller than the poststall moments shown in Fig. 4. Finally, the incremental trim drag measured at an extreme flap deflection of $\delta_{\text{flap}} = 10$ deg reduced the L/D ratio (at $\alpha = 6$ deg) to 24.65, from 27.9 at zero flap deflection, demonstrating only moderate penalty in configuration efficiency caused by excessive trim.

Conclusions

Aerodynamic tailoring was used to demonstrate the performance of a lifting-body/wing configuration using a low-Reynolds-number test. A relatively high-camber airfoil shape was designed for the small-scale test so that wing stall would occur in the range expected of a full-scale aircraft. Wind-tunnel tests confirmed that the fuselage can be used as a simple and inexpensive high-lift device, demonstrating a maximum L/D value of 27.9. In addition, at high angles of attack the fuselage side-edge vortex lift creates a large nose-down pitching moment that can be used to obtain a stall-safe lifting-body configuration. Finally, from a theoretical point of view the aircraft model with the highly cambered airfoil can be seen as the low-speed configuration of a single element, adaptive (flexible) wing section, which transforms to a high-speed shape at cruise. Transition between the two airfoil shapes (in this particular case) would take place at about $\alpha = 4$ deg.

Acknowledgments

This work was partially supported by the Lockheed Martin/California State University Partnership Program. The authors also acknowledge the valuable advise provided by Robert Hahl during this study.

References

[1]Katz, J., Byrne, S., and Hahl, R., "Stall Resistance Features of Lifting-Body Airplane Configurations," AIAA Paper 98-0760, Jan. 1998; also *Journal of Aircraft*, Vol. 36, No. 2, 1999, pp. 471–474.

[2]Drela, M., "Design and Optimization Method for Multielement Airfoil Flow," AIAA Paper 93-0969, Feb. 1993.

[3]Ashby, L. D., Dudley, M. D., Iguchi, S. K., Browne, L., and Katz, J., "Potential Flow Theory and Operation Guide for the Panel Code PMARC," NASA TM 102851, March 1990.

[4]McMasters, J. H., and Kroo, I., "Advanced Configurations for Very Large Transport Airplanes," AIAA Paper 98-0439, Jan. 1998.

[5]Liebeck, R. H., Page, M. A., and Rawdon, B. K., "Blended-Wing-Body Subsonic Commercial Transport," AIAA Paper 98-0438, Jan. 1998.

Database Tomography Applied to an Aircraft Science and Technology Investment Strategy

Ronald N. Kostoff*
Office of Naval Research, Arlington, Virginia 22217-5660
Kenneth A. Green†
Titan Corporation, Warminster, Pennsylvania 18974
Darrell Ray Toothman‡
RSIS, Inc., McLean, Virginia 22102
and
James A. Humenik§
NOESIS, Inc., Manassas, Virginia 20104

I. Introduction

THIS Note summarizes the results of applying text data mining (TDM) techniques to aircraft science and technology (S&T) records retrieved from two source technology databases for the purpose of obtaining technical intelligence on aircraft S&T. A much more detailed presentation of the results and TDM techniques is contained in the study's final report.[1] Two complementary TDM techniques were used in this study: 1) bibliometrics to identify the infrastructure of aircraft S&T (e.g., who are the performers, where are the results archived, what are the seminal papers) and 2) computational linguistics to identify the main aircraft S&T thematic areas and the relationships of these thematic areas to each other and to the infrastructure. The source databases examined were the science citation index (SCI)[2] (basic research, 1991–1998) and the engineering compendex (EC)[3] (applied research/technology, 1990–1998). Records were retrieved from these databases using an iterative query technique and then examined using a patented software system for analyzing large amounts of textural material.[4,5]

Aircraft S&T, as defined here, consists of development of different aircraft/helicopter components or technologies to improve system performance or safety or to reduce costs. Use of aircraft for purposes other than platform S&T development, such as crop dusting or as an instrument platform for geophysical experiments, was typically excluded unless an extrapolation to improving military aircraft performance could be identified.

The final query used to retrieve records from the SCI contained 207 terms and is shown in Ref. 1. The final query used to retrieve records from the EC contained essentially the 13 terms preceding the NOT Boolean in the SCI query (aircraft or air vehicle* or helicopter* or rotorcraft or unmanned air vehicle or uninhabited combat air vehicle (UCAV) or vertical takeoff and landing or very short takeoff and landing or advanced short takeoff and vertical landing or short takeoff and vertical landing or avionic* or cockpit or aircrew*). Very few abstracts that were extraneous to the focus of the study were retrieved from the EC, and the EC database did not require the same number of iterations used for the SCI database. This derives from the fact that the platform technology focus of the study is better aligned with the platform technology orientation of the EC database than

Received 10 May 1999; revision received 1 April 2000; accepted for publication 24 April 2000. This material is declared a work of the U.S. Government and is not subject to copyright protection in the United States.

*Physical Science Administrator, Code 35, 800 North Quincy Street.
†Senior Member Technical Staff, Semcor Division.
‡Database Management Specialist, Code 61, 1651 Old Meodow Road, Suite 500.
§Senior Engineer, Code 35, 10530 Linden Lake Plaza, Suite 201.